An Initial Solution Based Selective Harmonic Elimination Method for Multilevel Inverter

Peeyush KALA, Abhinav SHARMA, Vibhu JATELY, Jyoti JOSHI, and Yongheng YANG

***Abstract*—This article presents an initial solution based selective harmonic elimination (SHE) method for multilevel inverter (MLI) that aims to solve SHE problem with high accuracy while significantly reducing the number of iterations. Initial SHE solution is defined as a set of initial switching angles that has less accuracy as compared to the final SHE solution. To find initial SHE solution, tunicate swarm algorithm (TSA), grey wolf optimization (GWO) and whale optimization (WO) are used to solve five-dimensional SHE problem. A comparative analysis demonstrates that TSA achieved the desired initial SHE solution within lesser iterations as compared to GWO and WO for a wide range of modulation indices. The initial switching angles found using TSA are further optimized using Newton-Raphson (NR) method being the proposed TSANR method, which exploits the SHE search space with quadratic rate of convergence to find final SHE solution. The proposed TSANR method significantly minimizes the computational time and further improves the accuracy of the SHE solution as compared to the state-of-the-art SHE methods. Detailed simulations, experimental and harmonic analysis under dynamic change in modulation index are presented to show the efficacy of the proposed SHE method in terms of control over fundamental and detrimental harmonics.**

***Index Terms*—Initial SHE solution, multilevel inverter, Newton-Raphson (NR), selective harmonic elimination (SHE), tunicate swarm algorithm (TSA).**

I. Introduction

MULTILEVEL inverters have shown their superiority over pulse width modulation (PWM) inverters in various industrial applications over the past few decades [1]. MLIs offer numerous key merits such as its transformer-less assembly, low total harmonic distortion (THD), reduced voltage stress in switches, and reduced switching losses, making them suitable for medium-voltage and high-power applications including standalone and grid-connected renewable energy systems (RES) [2]–[3]. The output voltage waveform of MLIs is a staircase AC waveform consisting of dominant low order harmonics such as 5th, 7th, 11th and 13th above the limits prescribed in IEEE 519-2014 standard. Hence, in order to minimize these harmonics and obtain the desired fundamental voltage for RES applications, researchers have applied selective harmonic elimination (SHE) techniques in MLIs [4]. In the SHE technique, special iterative methods such as numerical methods, metaheuristic approaches, and algebraic methods are required to solve the multi-dimensional nonlinear transcendental equations at a chosen modulation index, M, simultaneously. Moreover, if the MLI has large number of voltage levels (the dimension of the SHE problem is very high), this might require much more computations and also large memory storage. The SHE solution provides optimum firing angles for a quarter fundamental cycle. Numerical methods such as Newton-Raphson (NR) are well defined mathematically and simple to program. It has a high convergence speed, if a good initial solution is provided. However, the performance of NR method is governed by appropriate selection of the initial solution for a wide range of M, thereby limiting its direct application in SHE problems [5]. Some of the researchers have proposed algebraic methods such as the theory of resultants, Groebner bases, and polynomial-based methods to solve SHE equations [6]–[7]. However, these methods increase the mathematical and computational burden of the processor for solving high dimension SHE problems. In [8], the homotopy perturbation based SHE method is proposed to reduce the number of iterations but at the cost of increased coding complexity. In [9], the authors used proportional and integral control for SHE problems. However, it could only minimize the 3rd and 5th harmonics.

The aforementioned limitations of numerical and algebraic SHE methods have led the attention of researchers to opt for metaheuristic techniques based SHE methods [10]. Metaheuristics are nature-inspired high-level search algorithms that offer advantages such as simplicity, flexibility, derivative-free mechanism that easily discover global optimal solutions for various complex engineering problems. In [11]–[12], authors used the genetic algorithm (GA) for harmonic mitigation in reduced component count multilevel inverters. However, GA consumes much time and is difficult to program as it requires operators such as crossovers, mutations and

Manuscript received June 21, 2023; revised August 22, 2023 and November 6, 2023; accepted December 18, 2023. Date of publication March 30, 2024; date of current version January 2, 2024. No funding was received to assist with the preparation of this manuscript. *(Corresponding author: Vibhu Jately.)*

P. Kala is with Department of Electrical and Electronics Engineering, SRM Institute of Science and Technology, Delhi-NCR Campus, Ghaziabad 201204, India (e-mail: peeyushk@srmist.edu.in).

A. Sharma is with the Department of Electrical and Electronics Engineering, University of Petroleum and Energy Studies (UPES), Dehradun 248007, India (e-mail: abhinavgbpuat@gmail.com).

V. Jately is with the School of Computer Science, University of Petroleum and Energy Studies (UPES), Dehradun 248007, India (e-mail: vibhujately@gmail.com).

J. Joshi is with Department of Computer Science and Engineering, Graphic Era Hill University, Dehradun 248002, India (e-mail: jjyotij25@gmail.com).

Y. Yang is with College of Electrical Engineering, Zhejiang University, Hangzhou 310027, China (e-mail: yoy@zju.edu.cn).

Digital Object Identifier 10.24295/CPSSTPEA.2023.00049

selections. In [13]–[14], the authors implemented particle swarm optimization (PSO)-based SHE methods for harmonic minimization in MLIs. It was found that PSO often prematurely converges to local minima when the dimension of the SHE problem increases. In [15], the Bee algorithm (BA) was used for harmonic minimization in a seven-level inverter. However, the tuning of various parameters in the proposed method is challenging. In [16]–[17], the researchers proposed a colonial competitive algorithm (CCA) and enhanced CCA for solving the SHE problem. However, the sensitivity analysis-based tuning of imperialistic fraction, rate of revolution, penetration rate, and advent rate is tedious. In [18], authors proposed a teaching–learning–based optimization (TLBO) method for solving the SHE problem in five-level and nine-level inverters, but the proposed method requires a higher number of iterations. In [19], the authors proposed a flower pollination algorithm (FPA) based SHE method with improved search ability. However, the proposed method has slow convergence during the exploitation stage and low search precision.

Recently, some researchers applied modified and hybrid metaheuristics based SHE techniques to overcome the above-mentioned drawbacks. In [20], the authors implemented a modified PSO technique using a mesh adaptive direct search and mutation strategy. Although, it improved the convergence rate and accuracy as compared to PSO and GA, but with increased coding complexity. In [21], authors proposed a modified fish swarm optimization (FSO) method to maintain balance between exploration and exploitation for eliminating the dominant harmonics in seven-level inverter. The method uses several new parameters, which increase the coding complexity and require a large number of iterations. In [22], the authors suggested an exponentially decaying function as a position coefficient for chaotic search based grey wolf optimization (GWO) to improve the search efficiency of the algorithm. However, evaluation of chaotic sequences is done using iterative methods, which increase the computational time. In [23], the authors have combined quantum bat algorithm (QBA) and opposite-based learning theory to improve the speed of convergence. However, the results of the modified QBA do not exhibit significant improvement as compared to other metaheuristic algorithms for the higher dimensional SHE problem. In [24], the authors proposed a hybrid metaheuristic algorithm, which combines the features of the gravitational search algorithm (GSA) and PSO to solve the SHE problem. The hybridization of GSA and PSO increases the number of parameters and results in large memory requirement. In [25], the authors implemented an asynchronous PSO-GA technique for SHE in seven-level inverter where an asynchronous PSO method was utilized for exploration while GA is used for exploitation. The technique requires fine tuning of various PSO and GA parameters for optimum results. In [26], the authors proposed a hybrid PSO-Tabu Search (TS) method to enhance the global search capability of the SHE solution. However, it requires a large number of iterations to find the optimum solution. In [27], the authors proposed the random PWM SHE method with master-slave mode to control the fundamental and sub-harmonics in (MPUC) inverter. Though, it reduced the percentage THD significantly, it operates at high switching frequency range (7000 Hz) which results in high switching losses. In [28], the researchers compared and analyzed the performance of SHE PWM and central 60-degree modulation on the traction system. It is found that THD value is comparatively larger as compared to the THD obtained in central 60-degree modulation technique. In [29], authors proposed an improved PSO method to mitigate the undesirable harmonics along with achieving the neutral point balancing under low-voltage ride-through (LVRT) condition. In conventional SHE method, THD rises for low values of M in variable load voltage application. To solve this problem, the researchers employed the dc-dc converter to achieve variable dc voltage and applied PSO SHE method to compute optimum switching angles [30]. M. Khizer *et al*. utilized the adaptive nature of enhanced firefly method to solve SHE problem [31]. In [32], authors proposed an improved SHE-PAM method to minimize the lower-order harmonic in 3-phase CHB MLI to meet the grid code standards by utilizing the half-wave symmetry.

M. Sharifzadeh *et al*. hybridized the SHE-PWM and SHM-PWM techniques to effectively mitigate the targeted harmonics while reducing the common mode voltage in the three-phase three-level inverter [33]. In [34], authors reviewed the various SHM techniques which were combined with MPC strategies to improve the compliance to the grid codes in steady state as well as in dynamic and transient conditions. In [35], the researchers implemented a hybrid modulation method by combining PS-PWM and asymmetric SHM PWM to reduce the harmonics within the limits defined in *IEEE-519-2014* for grid connected CHB MLI. In [36], authors examined the performance of Bat algorithm based SHE and SHM techniques on the compact nine-level switched-capacitor inverter. Authors in [37] analysed the performance of the SHM technique on CHB MLI for PMSM drive application. In [38], researchers devised a SHM-PWM method to provide control over THD and harmonics under unequal dc-link voltages. Real-time implementation of the SHM-PWM technique is a key challenge due to the necessity of solving nonlinear transcendental Fourier equations. Therefore, authors presented a deep learning method based SHCM-PWM technique for grid-tied CHB MLI in the real-time environment [39]. GSA is used to solve SHE problem in [40]. In [41], researchers presented a general mathematical solution to solve SHE problem for MLI with both symmetrical and unsymmetrical dc sources. In [42], the authors proposed the homotopy perturbation based SHE method to compute optimum switching angles with very fast convergence rate. A comparison is carried out between the recent SHE and SHM techniques as in Table I. It can be summarized from Table I that the existing state-of-the-art SHE and SHM methods can mitigate the selected dominant harmonics and can effectively reduce the line THD. However, these methods consume considerably much higher number of iterations to solve SHE/SHM problem.

From the above discussion, it is evident that researchers have used hybrid metaheuristic SHE and SHM methods to increase the accuracy of SHE solution and reduce the

TABLE I
LITERATURE SURVEY OF SHE AND SHM TECHNIQUES

Scheme	Algorithm	Frequency range	Voltage waveform pattern	Minimum line THD	Harmonics mitigated	Iterations required
SHE	Enhanced firefly [31]	Low	HWS	4.7 %	5th , 7th, 11th	100
	Hybrid PSO-TS algorithm [26]	High	HWS	6.19%	5th, 7th, 11th, 13th, 17th, 19th , 23rd	500
	PSO-optimized SHE [30]	High	HWS	12.23%	3rd to 29th	-
	Bat Algorithm [36]	Low	QWS	9.81%	3rd, 5th , 7th and 9th	500
	Hybrid GSA [24]	Low	QWS	8.6 %	5th, 7th, 11th	200
	APSOGA [25]	Low	QWS	11.47%	3rd, 5th	200
	TLBO [18]	High	QWS	-	3rd, 5th	2000
SHM	Hybrid SHM-PWM [33]	Low	QWS	34.30%	5th, 7th, 11th, 13th, 17th, 19th , 23rd	3000
	improved SHM-PAM [32]	Low	HWS	4.23%	5th, 7th, 11th, 13th, 17th, 19th , 23rd, 25th	100
	Bat Algorithm- SHM [36]	Low	QWS	7.62%	3rd, 5th , 7th and 9th	500
	Hybrid SHM SHE PAM [38]	Low	QWS	10%	5th to 23rd	-

number of iterations by maintaining balance between the rate of exploration and exploitation. However, one of the major drawbacks is that these methods require a large number of well-tuned parameters increasing the coding complexity. Moreover, these parameters require a large memory space of the controller and higher number of iterations to obtain the optimum SHE solution. Due to these limitations, there is a need to introduce a simple and fast convergence SHE method. Therefore, an initial SHE solution based approach is proposed in this paper.

The proposed method is essentially divided into two stages. In the first stage, a recently developed tunicate swarm algorithm (TSA) is used to obtain an initial solution for the SHE problem as a set of switching angles. In the latter stage, this initial solution is further improved using the NR method to quickly obtain the optimized final solution. TSA has superior performance over other metaheuristic techniques like GA, PSO, GSA, spotted hyena optimizer (SHO), GWO, sine-cosine algorithm, and emperor penguin optimizer in solving multimodal benchmark functions [43]. The convergence analysis of the TSA reveals that it does not get stuck in local optima. Hence, TSA is preferred over other metaheuristic methods to determine the initial switching angles for SHE problem. Once the initial switching angles are determined, these are further refined using the NR SHE method. The proposed method, namely TSANR method, combines the benefits of TSA and NR method while overcoming their deficiencies. The TSANR SHE method requires tuning of fewer parameters, reduced number of iterations, and hence, less computational time, reduced level of complexity and memory space. The key novelty of the proposed work includes:

- The concept of initial and final SHE solutions to develop a fast TSANR method and its performance analysis;
- Comparison of the TSANR method with state-of-the-art metaheuristics SHE methods;
- Implementation of the proposed TSANR SHE method on an eleven-level MLI topology.

The rest of the manuscript is as follows: Section II explains the concept of initial and final SHE solution for the foundation of the proposed SHE method. In Section III, the proposed TSANR SHE method is discussed along with the mathematical steps involved in determining the optimum SHE solution. Section IV provides the rationale behind using TSA to determine the initial SHE solution. Section V establishes the superior performance of the TSANR method on the basis of the convergence speed and accuracy. Section VI provides the simulation results under constant and sudden change in *M*. Section VII provides the experimental results to validate the performance of the TSANR SHE method under dynamic change in modulation index. Section VII concludes the study and outlines the benefits of the proposed SHE method. prepare your manuscript.

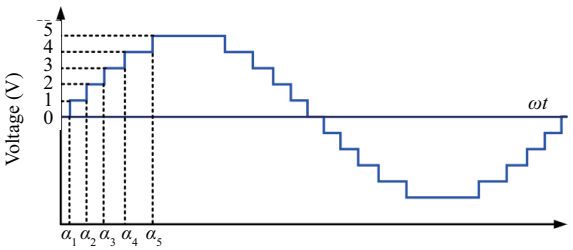

Fig. 1. 11-level voltage waveform of MLI.

II. STATEMENT OF RESEARCH PROBLEM

Fig. 1 shows the output voltage waveform of an 11-level MLI, which exhibits quarter-wave symmetry. There are five switching angles α_1, α_2, α_3, α_4, and α_5 in the range 0 to $\pi/2$ radians which can be found using the SHE technique. The mathematical expression of this load voltage waveform is expressed as

$$v(\omega t) = \frac{4V}{\pi} \sum_{n=1,3,5}^{\infty} \frac{1}{n} \sin(n\omega t) \sum_{i=1}^{5} [k_i \cos(n\alpha_i)] \qquad (1)$$

where, n represents nth harmonic, i represents the dimension of the SHE problem, k_i represents the multiplier for ith dc source. This multiplier is equal for identical dc voltage sources and are unequal if there is small variation in dc voltage sources. Therefore, the magnitude of dc sources is represented as

$$V_1 = k_1 V,\ V_2 = k_2 V,\ V_3 = k_3 V,\ V_4 = k_4 V,\ V_5 = k_5 V \qquad (2)$$

The actual amplitude of fundamental voltage present in this waveform can be represented by (3), while (4) represents the desired fundamental voltage.

$$V_1 = \frac{4V}{\pi}[k_1\cos(\alpha_1) + k_2\cos(\alpha_2) + ... + k_5\cos(\alpha_5)] \quad (3)$$

$$V_{1d} = \frac{4 \cdot V \cdot M \cdot (k_1 + k_2 + k_3 + k_4 + k_5)}{\pi} \quad (4)$$

The amplitude of 5th, 7th, 11th, and 13th harmonic voltages are given in (5)–(8), respectively.

$$V_5 = \frac{4V}{5\pi}\sum_{i=1}^{5}[k_i\cos 5\alpha_i] \quad (5)$$

$$V_7 = \frac{4V}{7\pi}\sum_{i=1}^{5}[k_i\cos 7\alpha_i] \quad (6)$$

$$V_{11} = \frac{4V}{11\pi}\sum_{i=1}^{5}[k_i\cos 11\alpha_i] \quad (7)$$

$$V_{13} = \frac{4V}{13\pi}\sum_{i=1}^{5}[k_i\cos 13\alpha_i] \quad (8)$$

The SHE technique is essentially divided into two objectives. The first objective is to maximize the actual fundamental voltage to the desired fundamental voltage level as in (9), whereas the second objective aims to eliminate the dominant 5th, 7th, 11th, and 13th harmonic voltages as in (10). To solve the SHE problem using metaheuristic technique, the fitness function as in (11) should be minimzed.

$$V_1 = V_{1d} \quad (9)$$

$$V_5 = V_7 = V_{11} = V_{13} = 0 \quad (10)$$

$$f = \min_{\alpha_i}\left\{\left[100\frac{(V_{1d} - V_1)}{V_{1d}}\right]^4 + \frac{1}{4}\sum_{h=5,7,11,13}\frac{1}{h}\left(100\frac{V_h}{V_1}\right)^2\right\} \quad (11)$$

The first term of the SHE fitness function represents the minimization of percentage errors in the amplitude of the fundamental voltage while other terms represent the minimization of 5th, 7th, 11th and 13th order harmonics. This function provides strict control over the fundamental component and detrimental harmonics. The lowest value of this function is desirable as it leads to an accurate solution of the SHE problem. However, metaheuristics based SHE techniques consume a large number of iterations to find final optimum SHE solution. Also, these may usually get trapped in a local minima solution, which reduces the accuracy of the SHE solution. In order to alleviate these limitations, an initial SHE solution based approach is introduced and analyzed in the subsequent sub-sections.

A. Initial SHE Solution

Initial SHE solution is a set of switching angles (α_1, α_2, α_3, α_4, and α_5) for which 5th , 7th, 11th, and 13th harmonics is below 3% as per *IEEE 519-2014* standard while the error in the fundamental voltage is set at 1%. Using these conditions in (11), we can find the initial value of the SHE fitness function at a given modulation index. The percentage error in the fundamental voltage for the initial SHE function is expressed as

$$\left(\frac{V_1 - V_1^d}{V_1^d}\right) \times 100 = 1 \quad (12)$$

Since the value of 5th, 7th, 11th and 13th harmonics should be less than 3% as per *IEEE 519-2014* standard, it is selected as 2% (nearest integer value < 3) for finding the initial value of the fitness function. Hence, the desired values of 5th , 7th , 11th and 13th harmonics are expressed as in (13)–(16).

$$\frac{V_5}{V_1} \times 100 = 2 \quad (13)$$

$$\frac{V_7}{V_1} \times 100 = 2 \quad (14)$$

$$\frac{V_{11}}{V_1} \times 100 = 2 \quad (15)$$

$$\frac{V_{13}}{V_1} \times 100 = 2 \quad (16)$$

The threshold value of the fitness function, $f_{\text{initial}} = 1.51$, is obtained by substituting (12)–(16) into (11). The initial SHE solution corresponds to a set of switching angles for which the value of fitness function "f" is less than or equal to the threshold value. By using a suitable metaheuristic technique, the initial SHE solution can be quickly determined within fewer iterations without getting trapped into local minima.

B. Final SHE Solution

To improve the accuracy of the initial SHE solution, a fast convergence iterative method is used to determine the optimized final SHE solution. The final SHE solution has higher accuracy as compared to the initial SHE solution as it completely eliminates the 5th, 7th, 11th, and 13th harmonics and the error in fundamental voltage. The final value of SHE fitness function is in the order of 10^{-30} reflecting the high accuracy of the proposed approach.

III. Proposed TSANR SHE Method

The proposed TSANR SHE method is an initial SHE solution based method, which aims to utilize the benefits of simple metaheuristic techniques, TSA and NR methods, together to find the optimum SHE solution. Kaur *et al*. [43] recently proposed a bio-inspired TSA, which is inspired from the swarm and jet propulsion behavior of tunicates. These are the members of subphylum tunicate, which are also referred to as sea squirts. Tunicates are identified from many meters through their bio-luminescent body emitting pale blue-green light. These have barrel like structure where water enters from one end and ejects from the other end and allows them to exhibit jet propulsion behavior, as shown in Fig. 2.

Tunicates search for food in deep oceans through jet propulsion behavior and with swarm intelligence all tunicates optimize their position with respect to the position of the best tunicate. The key feature of the TSA is that it avoids conflict

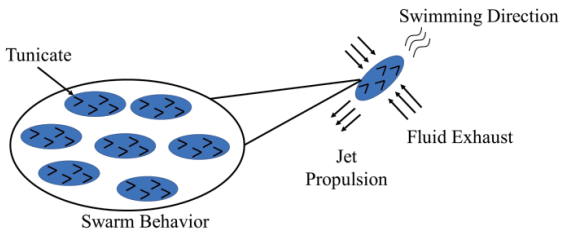

Fig. 2. Tunicate swarm optimization algorithm [43].

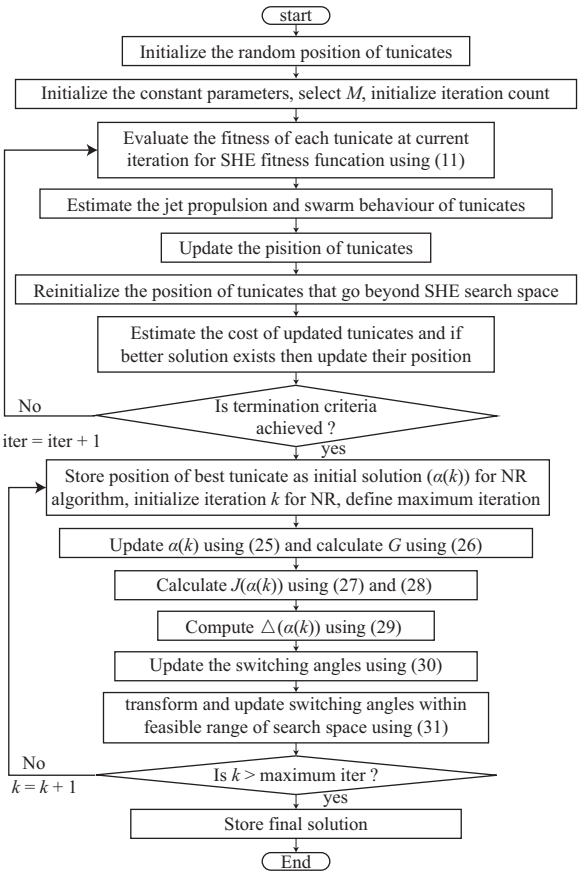

Fig. 3. Flow chart of the proposed TSANR algorithm.

among search agents and also allow movement of search agents toward the direction of the best agent. Since TSA has a faster convergence rate at early iterations while slower rate of convergence at later iterations, it is desirable to hybridize TSA with NR, a fast-converging iterative method to solve the SHE problem. The flowchart of the proposed SHE method is shown in Fig. 3.

The mathematical model of the proposed TSANR SHE method is outlined in the following steps:

Step 1: Randomly initialize the population of N tunicates (search agents) in the SHE search space which is between 0 to $\pi/2$ radians. Position of the pth tunicate in the SHE search space is defined as:

$$X_p = (X_p^1, X_p^2, ..., X_p^i, ..., X_p^n) \quad \text{for } i = 1,2,...,n. \tag{17}$$

where, i denotes ith dimension of SHE function and X_p^i is position of pth tunicate in the ith dimension of SHE search space.

Step 2: Introduce the constant parameter $\vec{A}$ as in (18) to avoid clash between search agents. It is defined as the ratio of gravity force ($\vec{G}$) to social force $\vec{M}$. (19) defines $\vec{G}$ where $\vec{F}$ represents the water flow advection in deep ocean as in (20). The expression of $\vec{M}$ is given in (21).

$$\vec{A} = \frac{\vec{G}}{\vec{M}} \tag{18}$$

$$\vec{G} = c_2 + c_3 - \vec{F} \tag{19}$$

$$\vec{F} = 2\,c_1 \tag{20}$$

$$\vec{M} = [X_{\min} + c_1 (X_{\max} - X_{\min})] \tag{21}$$

where c_1, c_2, c_3 are random numbers in the range [0, 1], $X_{\min}$ and $X_{\max}$ are the initial and subordinate speeds considered as 1 and 4 respectively which are introduced to enable social interaction.

Step 3: Examine the fitness of search agents by placing their position in the SHE fitness function as in (11).

Step 4: Determine the position of best search agent in the SHE search space.

Step 5: Examine the jet propulsion and swarm behavior of search agents and find $\vec{PD}$ as

$$\vec{PD} = \left| \vec{FS} - \text{rand}\, \vec{X}_p\,(x) \right| \tag{22}$$

where, $\vec{PD}$ is the total distance between the tunicate and food source, rand is a random number in the range [0, 1], x indicates the current iteration, $\vec{FS}$ indicates the position of food source, $\vec{X}_p\,(x)$ is the position of search agent which is defined as

$$\vec{X}_p(x) = \begin{cases} \vec{FS} + \vec{A}\ \vec{PD}, \text{if rand} \geqslant 0.5 \\ \vec{FS} - \vec{A}\ \vec{PD}, \text{if rand} < 0.5 \end{cases} \tag{23}$$

The position of all search agents is updated with respect to the position of two tunicates having lowest fitness value and update the position of each search agent using (24).

$$\vec{X}_p\,(x+1) = \frac{\vec{X}_p\,(x) + \vec{X}_p\,(x+1)}{2 + c_1} \tag{24}$$

Step 6: Determine the search agents whose position lies beyond the defined search space and reinitialize their position within the SHE search space.

Step 7: Evaluate the fitness value of the updated search agent and update its position if the new solution is better than the previous one.

Step 8: If the initial solution is reached or maximum number of iterations is accomplished, the algorithm ends. Otherwise, repeat Steps 5 to 8.

Step 9: Initialize iteration count k for NR algorithm. Initial switching angles are saved in row vector $\alpha(k)$. It consists of five switching angles at iteration $k = 1$ for chosen value of M:

$$\alpha(k) = [\alpha_1(k) \;\; \alpha_2(k) \;\; \alpha_3(k) \;\; \alpha_4(k) \;\; \alpha_5(k)] \tag{25}$$

Step 10: Five SHE equations shown in (9)–(10) are transformed in the form of a column vector G as in (26). The first row of G represents fundamental voltage error at kth iteration while the second, third, fourth and fifth row represents the actual magnitude of 5th, 7th, 11th and 13th harmonics at kth iteration for the selected M. The objective of the proposed SHE is to minimize the values of $g_1,...,g_5$ following the iterative procedure which is a function of $\alpha(k)$.

$$G = \begin{bmatrix} k_1\cos\alpha_1(k) + \cdots + k_5 cos\alpha_5(k) - M(K_1 + K_2 + \cdots + K_5) \\ k_1\cos 5\alpha_1(k) + k_1\cos 5\alpha_2(k) + \cdots + k_5\cos 5\alpha_5(k) \\ k_1\cos 7\alpha_1(k) + k_1\cos 7\alpha_2(k) + \cdots + k_5\cos 7\alpha_5(k) \\ k_1\cos 11\alpha_1(k) + k_1\cos 11\alpha_2(k) + \cdots + k_5\cos 11\alpha_5(k) \\ k_1\cos 13\alpha_1(k) + k_1\cos 13\alpha_2(k) + \cdots + k_5\cos 13\alpha_5(k) \end{bmatrix} = \begin{bmatrix} g_1 & g_2 & g_3 & g_4 & g_5 \end{bmatrix}^{\mathrm{T}} \tag{26}$$

Step 11: Compute the Jacobian matrix $J(\alpha(k))$ as

$$J(\alpha(k)) = \begin{bmatrix} \frac{\partial g_1}{\partial \alpha_1} & \frac{\partial g_1}{\partial \alpha_2} & \frac{\partial g_1}{\partial \alpha_3} & \frac{\partial g_1}{\partial \alpha_4} & \frac{\partial g_1}{\partial \alpha_5} \\ \frac{\partial g_2}{\partial \alpha_1} & \frac{\partial g_2}{\partial \alpha_2} & \frac{\partial g_2}{\partial \alpha_3} & \frac{\partial g_2}{\partial \alpha_4} & \frac{\partial g_2}{\partial \alpha_5} \\ \frac{\partial g_3}{\partial \alpha_1} & \frac{\partial g_3}{\partial \alpha_2} & \frac{\partial g_3}{\partial \alpha_3} & \frac{\partial g_3}{\partial \alpha_4} & \frac{\partial g_3}{\partial \alpha_5} \\ \frac{\partial g_4}{\partial \alpha_1} & \frac{\partial g_4}{\partial \alpha_2} & \frac{\partial g_4}{\partial \alpha_3} & \frac{\partial g_4}{\partial \alpha_4} & \frac{\partial g_4}{\partial \alpha_5} \\ \frac{\partial g_5}{\partial \alpha_1} & \frac{\partial g_5}{\partial \alpha_2} & \frac{\partial g_5}{\partial \alpha_3} & \frac{\partial g_5}{\partial \alpha_4} & \frac{\partial g_5}{\partial \alpha_5} \end{bmatrix} \tag{27}$$

Step 12: Calculate the differential correction in angles $\Delta(\alpha_k)$ for the next iteration using (29). NR method uses this term to update the switching angle for the next iteration $(k + 1)$.

$$J = \begin{bmatrix} -\sin(\alpha_1(k)) - \sin(\alpha_2(k)) - \sin(\alpha_3(k)) \ldots - \sin(\alpha_5(k)) \\ -5\sin(5\alpha_1(k)) - 5\sin(5\alpha_2(k)) \ldots - 5\sin(5\alpha_5(k)) \\ -7\sin(7\alpha_1(k)) - 7\sin(7\alpha_2(k)) \ldots - 7\sin(7\alpha_5(k)) \\ -11\sin(11\alpha_1(k)) - 11\sin(11\alpha_2(k)) \ldots - 11\sin(11\alpha_5(k)) \\ -13\sin(13\alpha_1(k)) - 13\sin(13\alpha_2(k)) \ldots - 13\sin(13\alpha_5(k)) \end{bmatrix} \tag{28}$$

$$\Delta(\alpha(k)) = -J^{-1}G \tag{29}$$

Step 13: Update the switching angles for the next iteration:

$$\alpha(k+1) = \alpha(k) + \Delta(k) \tag{30}$$

Step 14: Perform a transformation to bring the switching angles in the feasible range of SHE search space, i.e., $\alpha = [0, \pi/2]$ using

$$\alpha(k+1) = \cos^{-1}(|\cos(\alpha(k+1))|) \tag{31}$$

Step 15: Update the switching angles with respect to Step 14 and calculate $\Delta(\alpha(k))$.

Step 16: Check whether $\Delta(\alpha(k))$ is less than the tolerance value. To increase the accuracy of the solution, ε is chosen equal to 10^{-30}. If the solution has reached the desired tolerance level, then save the final switching angles in the lookup table. Else, increase the count of k by one and go to Step 9 and repeat the process from Steps 9 to 16.

Step 17: Store the final optimum SHE solution.

Although the SHE methods are usually implemented offline, the online implementation of the proposed SHE method can also be carried out.

The steps for the real-time implementation of the proposed SHE method is given below [38]:

(i)The proposed SHE method pre-calculates the optimum switching angles for selected value of M by solving non-linear transcendental equations.

(ii)These switching angles for each value of M will be stored in the lookup table.

(iii)The stored switching angles for chosen values of M are fetched to the switching control algorithm made in the MATLAB/Simulink platform. This switching control algorithm with lookup table is downloaded on real-time controller.

(iv)The real-time controller generates the switching pulses for the twelve switches of MLI according to the desired value of M and thus, the desired value of output voltage. These pulses are extracted from the digital I/O ports of controller to the gate driver ICs which will turn ON and OFF the MOSFET switches.

IV. Rationalization of TSA for Initial SHE Solution

This section investigates the performance of TSA in solving the SHE problem when compared with recently developed GWO and WO SHE method. The comparison is carried out based on the number of iterations and the accuracy of the method to obtain the initial SHE solution. Moreover, the effect of the initial SHE solution on the desired fundamental voltage and detrimental harmonics is carried out for TSA to demonstrate its effectiveness over GWO and WO SHE method.

A. Comparison of TSA With Prior-Art SHE Methods

In the first case study, exploration and exploitation abilities of TSA are analysed against GWO and WO for 500 iterations to solve the five dimensional SHE fitness function, where the number of search agents are considered 30. The simulation is carried out 10 times for each modulation index and the mean fitness values are used for comparison. The comparative simulation results for two modulation indices, $M = 0.845$ and 0.45, are shown in Fig. 4(a) and (b), respectively. It can be seen in Fig. 4 that TSA explores the SHE search space at a faster rate of convergence during early iterations (upto 50 iterations) as compared to GWO and WO. This high rate of exploration of TSA is desirable for finding the initial SHE solution. However, it can be observed that the rate of exploitation of TSA, GWO

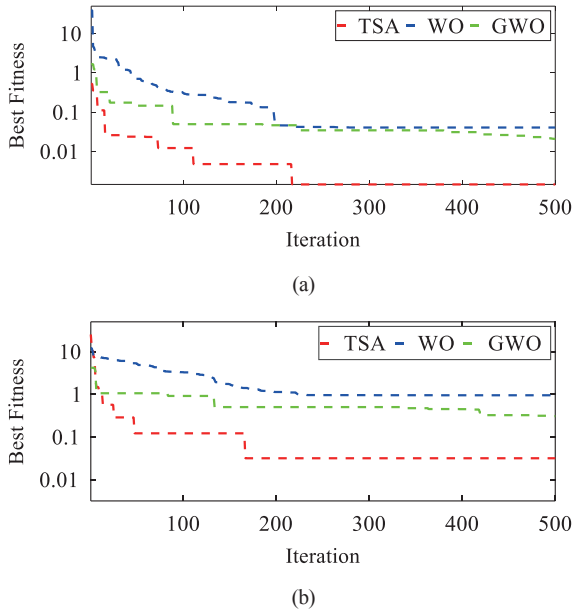

Fig. 4. Rate of convergence of TSA, GWO and WO on SHE fitness function at: (a) $M = 0.845$, and (b) $M = 0.45$.

and WO is slow during subsequent iterations thereby reducing the accuracy of the final SHE solution. The initial SHE solution is further elaborated in the following sub-section.

B. Convergence and Harmonic Analysis of Initial SHE Solution

In this section, convergence ability of TSA is compared against GWO and WO for finding the desired initial SHE solution for various values of M. To determine the initial SHE solution, the algorithms are run for 20 iterations and the corresponding results are shown in Fig. 5(a)–(d). For $M = 0.845$, TSA swiftly reaches below the threshold value of initial SHE solution within 3 iterations. On the other hand, GWO requires nearly 8 iterations and WO was unable to find the initial SHE solution as shown in Fig. 5(a). Similarly, for $M = 0.7$ and 0.6 TSA reached the threshold value of the initial SHE solution within 5 iterations as opposed to a large number of iterations taken by GWO to converge towards the threshold value as shown in Fig. 5(b) and (c). It is interesting to note that under a low value of modulation index at $M = 0.45$, GWO and WO failed to converge towards the initial SHE solution, whereas TSA quickly reached the threshold SHE value, as shown in Fig. 5(d). For a wide range of modulation indices, $M = 0.845$, 0.7, 0.6, 0.5, WO failed to find the initial SHE solution as it gets trapped into local minima as shown in Fig. 6. From the above discussion, it is obvious that TSA outperforms the other metaheuristic approaches in terms of the speed of convergence to reach the optimum value of the initial SHE solution.

Detailed simulation studies are carried out to investigate the effect of the initial SHE solution on the fundamental voltage as well as on the percentage value of 5th, 7th, 11th and 13th harmonics for a wide range of M using metaheuristic algorithms. The effect of the initial SHE solution obtained by the WO SHE method on the percentage error in the fundamental

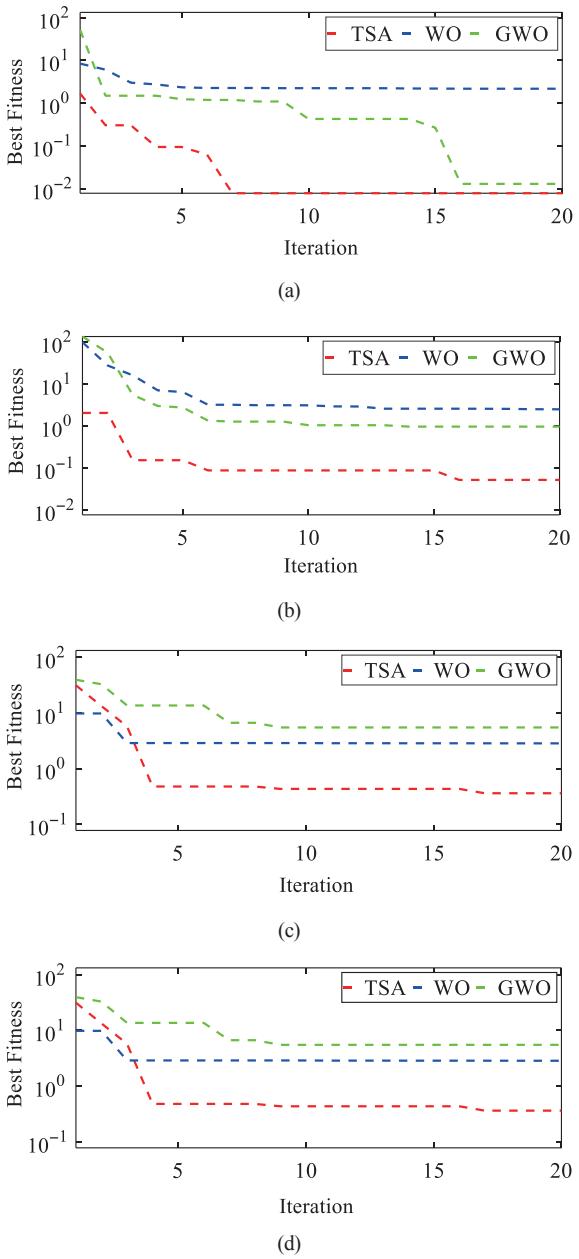

Fig. 5. Convergence response of metaheuristic techniques to find the initial SHE solution at: (a) $M = 0.845$, (b) $M = 0.7$, (c) $M = 0.6$, (d) $M = 0.45$.

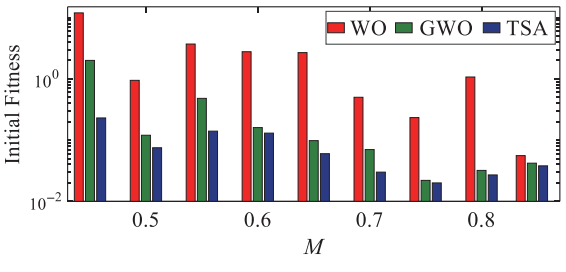

Fig. 6. Comparison of metaheuristic algorithms to find the accurate initial SHE solution.

voltage and the dominant harmonics is shown in Fig. 7(a). It can be seen in Fig. 7(a) that the harmonic percentage of the individual harmonics is above 3% for $M = 0.45$, 0.55, 0.6, 0.65,

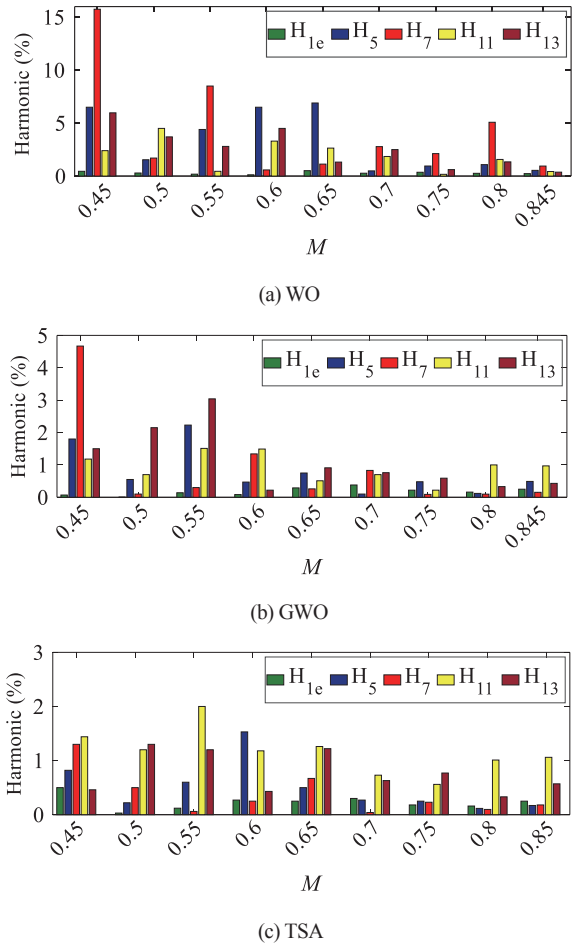

Fig. 7. Efficacy of metaheuristic techniques to suppress the dominant harmonics and error in the fundamental voltage.

TABLE II
INITIAL SWITCHING ANGLES USING TSA

M	α_1	α_2	α_3	α_4	α_5
0.845	0.1441	0.2118	0.4468	0.6186	1.0114
0.8	0.1344	0.3103	0.4872	0.7965	1.091
0.75	0.2189	0.3688	0.609	1.0166	1.0456
0.7	0.16559	0.4935	0.7399	0.9432	1.2693
0.65	0.3422	0.6214	0.8886	1.0529	1.2012
0.6	0.5110	0.7599	0.8882	1.0876	1.2666
0.55	0.3644	0.7208	0.9809	1.1094	1.511
0.5	0.6031	0.8037	0.9801	1.226	1.483
0.45	0.5969	0.8127	1.056	1.3128	1.5707

0.8. This is because WO is unable to reach the threshold value of the initial SHE fitness for the above-mentioned modulation indices. The percentage value of dominant harmonics and the percentage error in the fundamental voltage by GWO are shown in Fig. 7(b). It can be observed that GWO was unable to find the initial SHE solution at $M = 0.45$, where the 7th harmonic is greater than 3%. On the other hand, TSA effectively suppressed the individual harmonics and error in the fundamental voltage below 3% for wide range of M as shown in Fig. 7(c). This is because TSA does not get stuck in the local minima and resulted in converging below the threshold value of the initial SHE fitness function. Due to its superiority over WO and GWO,

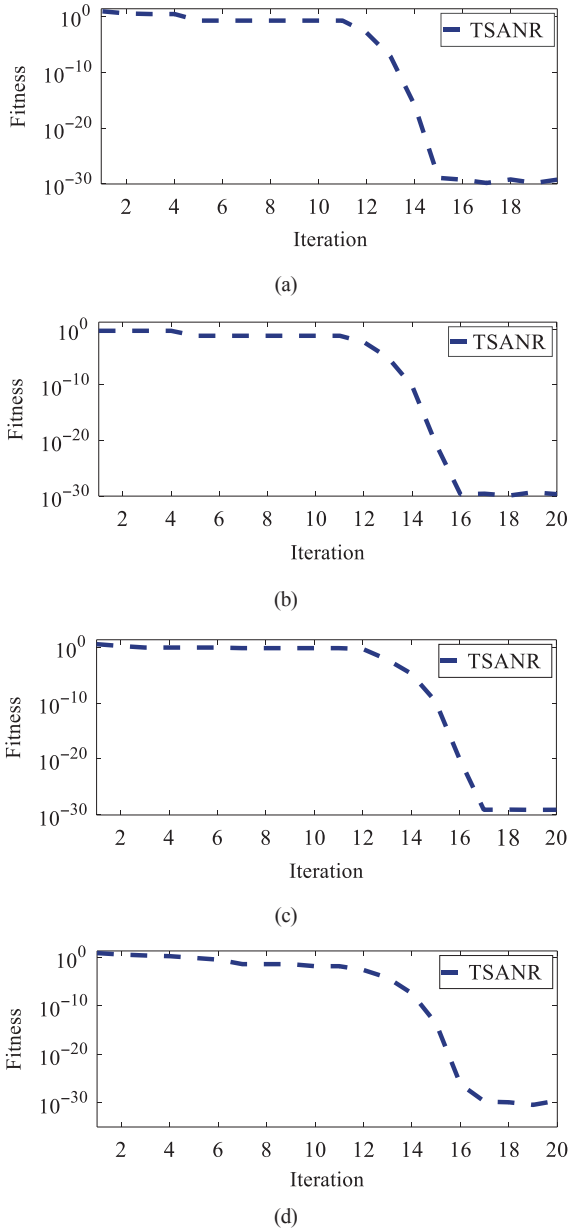

Fig. 8. Convergence plots of TSANR in reaching the final SHE solution for various modulation indices at: (a) $M = 0.45$, (b) $M = 0.6$, (c) $M = 0.7$ and (d) $M = 0.845$.

TSA is used to compute the initial switching angles, as given in Table II. The switching angles are expressed in radians for a quarter cycle.

V. PERFORMANCE EVALUATION OF TSANR SHE METHOD

Initial switching angles computed from TSA are used by the NR method, which aims to significantly improve the quality of the SHE solution. To evaluate the efficacy of the proposed method, simulations are carried out for 20 iterations for distinct modulation indices, as shown in Fig. 8(a)–(d). The initial switching angles are computed within the first ten iterations as mentioned in Steps 1 to 9 of the TSANR algorithm, while the NR method iteratively determines the optimum switching

TABLE III
FINAL SWITCHING ANGLES USING TSANR

M	F	α_1	α_2	α_3	α_4	α_5
0.845	7.3×10^{-32}	0.1451	0.2196	0.4202	0.6273	1.0039
0.8	1.8×10^{-30}	0.1146	0.3305	0.4744	0.7877	1.0863
0.75	4.5×10^{-30}	0.2233	0.3668	0.6251	0.9878	1.0702
0.7	8.5×10^{-30}	0.1438	0.5001	0.7209	0.9327	1.2808
0.65	8.4×10^{-31}	0.3411	0.6224	0.9037	1.0135	1.2158
0.6	1.3×10^{-31}	0.4649	0.7667	0.8994	1.0890	1.2654
0.55	7.6×10^{-30}	0.34186	0.6788	0.9851	1.1089	1.5396
0.5	1.6×10^{-30}	0.62009	0.79401	0.99843	1.20778	1.48219
0.45	3.5×10^{-30}	0.62176	0.83345	1.04865	1.31169	1.5609

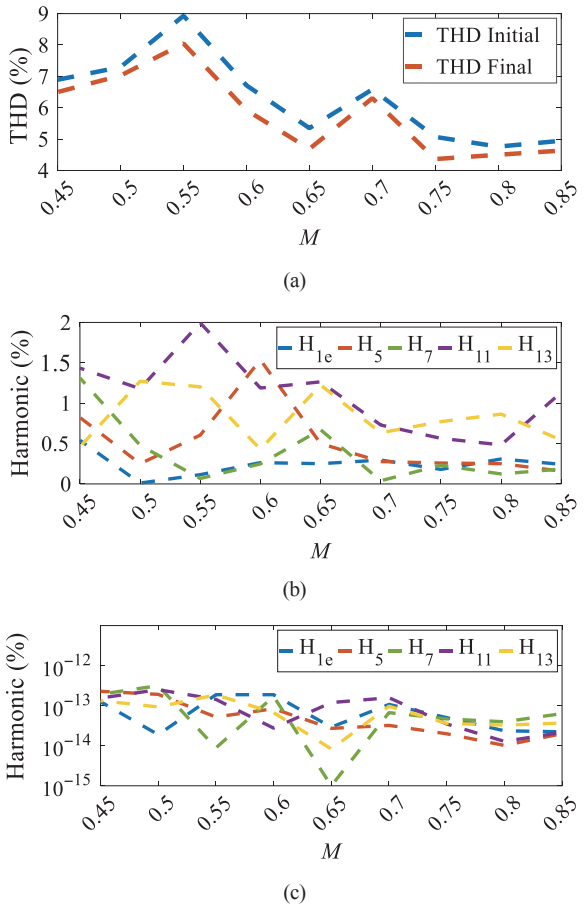

Fig. 9. Comparison between initial and final SHE solution under varying modulation index based on: (a) THD (%) using TSANR, (b) Percentage value of dominant harmonics and error in the fundamental voltage from the initial solution and (c) Percentage value of dominant harmonics and error in the fundamental voltage from the final solution using TSANR method.

angles in the remaining iterations. It is evident from the results that for the first ten iterations, the accuracy of the initial SHE solution is in the order of 10^{-1} to 10^{-2} and after 10th iteration, NR exploits the initial SHE solution at a quadratic convergence rate. Moreover, the proposed TSANR has the lowest value of SHE fitness function ($f < 10^{-30}$) and rapidly converged at the final SHE solution as compared to TSA, GWO, and WO SHE methods, as shown in Figs. 5 and 8. The final switching angles (radians) are computed using TSANR, as shown in Table III.

The effectiveness of the final SHE solution is demonstrated

TABLE IV
COMPARISON WITH RECENT METAHEURISTIC SHE

SHE method	Dimension	Fitness function	Iteration	Level of complexity	Memory required
TSANR	5	10^{-32}	20	Medium	Low
TLBO [18]	4	10^{-14}	2000	Medium	High
FPA [19]	6	10^{-19}	400	Medium	High
MPSO [20]	5	10^{-13}	300	High	High
PSFSO [21]	3	10^{-40}	200	High	High
OQBA [23]	5	10^{-4}	1000	High	High
HGSA [24]	4	10^{-15}	200	High	High
APSOGA[25]	4	10^{-11}	200	High	High
MGWO [44]	5	10^{-46}	200	High	High
WO [45]	5	10^{-6}	250	Low	Low

in terms of a reduced percentage THD and dominant harmonics, as shown in Fig. 9. The difference in the percentage THD for the initial and final SHE solution is shown in Fig. 9 (a).

It can be seen that the line THD values are significantly reduced with the final SHE solution. The percent error in the fundamental (H_{1e}) and dominant harmonics; 5th (H_5), 7th (H_7), 11th (H_{11}) and 13th (H_{13}) are computed using the initial SHE solution under varying modulation indices is shown in Fig. 9.

It is evident that the value of H_{1e} is well below 1% while percent values of harmonics H_5, H_7, H_{11} and H_{13} are below 2%. This confirms the effectiveness of the TSA in finding the appropriate initial SHE solution. The final SHE solution obtained using the NR method significantly reduces the percent value of the dominant harmonics below $10^{-12} \approx 0$ and the percent error in fundamental voltage, H1e is below $10^{-13} \approx 0$, as shown in Fig. 9(c). It can be observed that the final SHE solution drastically improves the harmonic profile of the output voltage waveform, as compared to the results obtained from the initial SHE solution as evident from Fig. 9(b) and (c). This is due to the hybridization of the TSA with NR method, which resulted in higher accuracy ($f < 10^{-30}$), as compared to low accuracy obtained from the initial SHE solution.

The proposed method is compared with the state-of-the-art metaheuristics like Teaching Learning Based Optimization (TLBO) [18], Flower Pollination Algorithm (FPA) [19], Modified Particle Swarm Optimization (MPSO) [20], Particle Swarm Fish Swarm Optimization (PSFSO) [21], Opposition-based Quantum Bat Algorithm (OQBA) [23], hybrid Gravitational Search Algorithm (GSA) [24], Asynchronous Particle Swarm Optimization-Genetic Algorithm (APSOGA) [25], modified Grey Wolf Optimization (GWO) [44], and Whale Optimization (WO) [45] based SHE methods to demonstrate the superiority of the proposed method based on some key performance indices. The performance indices chosen for comparison are the dimension of the SHE problem, fitness function value, number of iterations, level of complexity and the memory requirement of the SHE method, as given in Table IV.

The complexity level is directly dependent on the dimension of the SHE problem. The results indicate that TSANR, MPSO, OQBA, MGWO, and WO can solve five-dimensional SHE problem whereas PSFSO is able to solve low dimension SHE

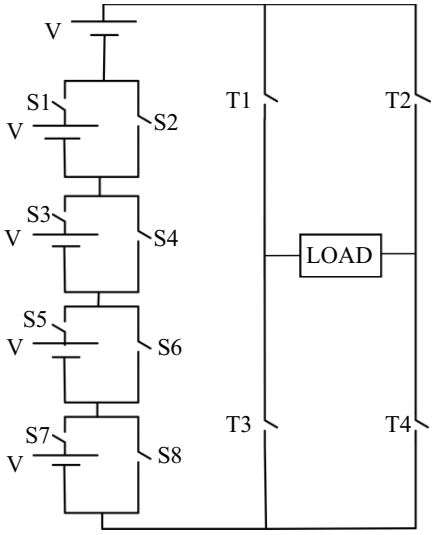

Fig. 10. 11-level MLI topology.

problem. Similarly, TLBO, HGSA, and APSOGA can solve four-dimensional SHE problem of low complexity.

The proposed TSANR method has the highest accuracy (lowest value of fitness function) as compared to TLBO, MPSO, OQBA, HGSA, APSOGA, and WO SHE methods to solve five-dimensional SHE problem. For 3-dimensional SHE problem, PSFSO achieved higher accuracy, as compared to the proposed SHE method. However, the 3-dimensional SHE problem has reduced degree of freedom which in turn can mitigate two dominant harmonics. The results indicate that the proposed SHE method converges to the lowest fitness value within 20 iterations as opposed to large number of iterations required by other state-of-the-art SHE methods. This confirms that TSANR considerably reduces the computation time for finding the optimum solution of the SHE problem. The hybridization of the TSA with NR method is of medium complexity and has low memory space requirement due to the reduced number of parameters and require the lowest number of iterations for convergence, as compared to other metaheuristics based SHE methods.

VI. Simulation Results

The performance of the proposed TSANR SHE method is implemented on a 11-level MLI under constant and dynamic change in M. To get the topological advantage over conventional CHB MLI topology, the TSANR SHE method is tested on a reduced component count (RCC) variable dc bus MLI whose working is explained in [46]. The circuit diagram of the 11-level MLI topology is shown in Fig. 10. The circuit consists of twelve switches and five identical dc sources as compared to twenty switches in the 11-level CHB topology. In the following subsections the simulation results are categorized under constant and dynamic change in M.

A. Under Constant M

In this study, the switching angles for M = 0.8 and M = 0.69 are computed using the proposed SHE method. For the simulation study, five dc sources of 12 V are chosen as input to the 11-level MLI with a single-phase load of R = 5 Ω and L = 20 mH. Fig. 11(a) shows the load voltage waveform at M = 0.8. Fig. 11(b) and (c) show the FFT analysis of load voltage and current waveforms, respectively. The results show that the 5th, 7th, 11th and 13th order harmonics are minimized in voltage and current waveforms while the overall THD is 6.8% and 0.61%, respectively. Fig. 11(d) show the output voltage waveform at M = 0.69. Fig. 11(e) delineates the harmonic analysis of the output voltage waveform. The dominant harmonics are effectively reduced and the maximum fundamental voltage is measured at 52.7 V with an overall THD of 14.74%. Hence, the proposed SHE method is able to evaluate the optimum firing angle of high precision which reduces the overall THD in the load voltage as well as maximizes the magnitude of the fundamental voltage.

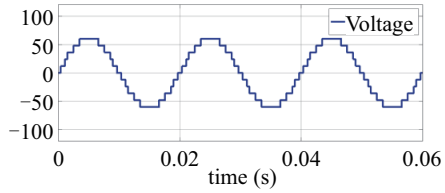

(a) load voltage waveform at M = 0.8

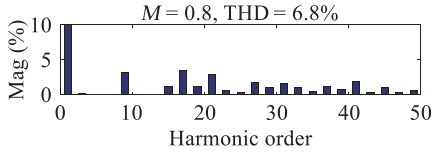

(b) FFT analysis of load voltage waveform at M = 0.8

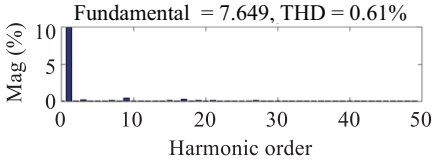

(c) FFT analysis of load current waveform at M = 0.8

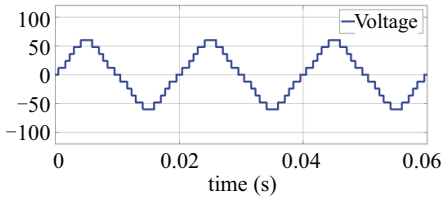

(d) load voltage waveform at M = 0.69

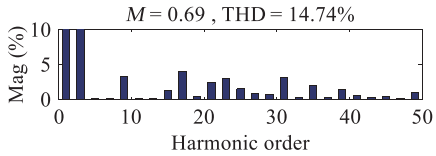

(e) FFT analysis of load voltage waveform at M = 0.69

Fig. 11. Simulation results of the load voltage waveform under different values of M.

B. Under Dynamic Change in M

In this study, the performance of the TSANR SHE method is examined under dynamic change in M. Several cases under dynamic change in M is considered to thoroughly examine the efficacy of the proposed SHE method.

In the first case, the modulation index is varied from $M = 0.78$ to 0.7 at $t = 0.06$ s. The load voltage and current waveforms are shown in Fig. 12(a). Fig. 12(b) and (c) show the THD value of 7.86% and 14.57% for voltage waveforms at $M = 0.78$ and 0.7, respectively. Fig. 12(d) and (e) show the THD value of 1.53% and 5% for current waveforms at $M = 0.78$ and 0.7, respectively. As evident from Fig. 12(a), the reduction in the peak value of the fundamental load voltage from 59.4 V to 53.4 V results in the slight reduction in the peak current from 7.4 A to 6.7 A, due to the decrease in M from 0.78 to 0.7, respectively.

In the second case, the modulation index is increased from $M = 0.7$ to 0.805 at $t = 0.06$ s. Fig. 12(f) shows an increment in the amplitude value of the fundamental voltage from 53.4 V to 61.4 V due to which the amplitude of the load current increases from 6.7 A to 7.8 A, as M increases from 0.7 to 0.805, respectively. Fig. 12 (g) and (h) show an improvement in the overall THD of the output voltage from 14.57% to 6.87% due to the increase in M.

In the last case, the modulation index is varied from $M = 0.845$ to 0.7 at the same time instant. The decrement in the peak value of the fundamental output voltage from 64.5 V to 53.4 V has a causal effect on the amplitude of the load current from 8.1 A to 6.7 A, due to the decrease in M from 0.845 to 0.7, respectively as shown in Fig. 12(i). The FFT analysis of the load voltage shows an increase in the THD from 8.79% to 14.57% due to the decrease in M, shown in Fig. 12(j) and (k). In Fig. 12(l) and (m), the FFT analysis of the load current waveforms are shown for this case study. It shows an increase in the THD from 2.49% to 5% due to the decrease in M from 0.845 to 0.7, respectively.

Fig. 12(a), (d), (g) shows negligible transient in the load voltage and current due to the high rate of convergence of the proposed TSANR method which is able to quickly evaluate the optimum firing angles under dynamic change in M. Moreover, the proposed method successfully eliminates the 5th, 7th, 11th and 13th harmonics while simultaneously maximizing the fundamental load voltage and effectively solves the SHE problem.

VII. Experimental Results

A lab-scale experimental prototype of an 11-level MLI is developed to validate the performance of the proposed SHE method. The dc sources are derived from five batteries with a nominal operating voltage of 12 V and a capacity of 80 Ah. The slight variation in the output voltage of the batteries is due to the inherent non-ideality and is given by $V_1 = 12.4$ V, $V_2 = 12.6$ V, $V_3 = 12.5$ V, $V_4 = 12.6$ V, $V_5 = 12.5$ V. The 11-level MLI assembly with the battery bank, controller circuit, load bank, digital storage oscilloscope TDS2024C, power quality

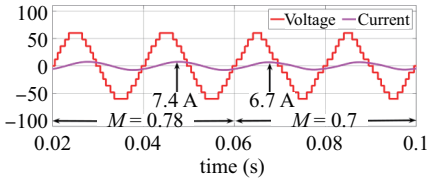

(a) voltage and current waveforms under sudden change in $M = 0.78$ to 0.7

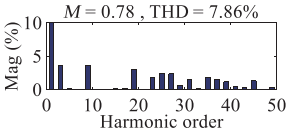

(b) FFT analysis of voltage at $M = 0.78$

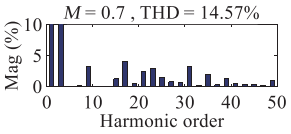

(c) FFT analysis at $M = 0.7$

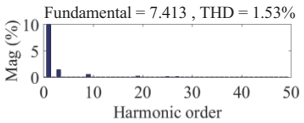

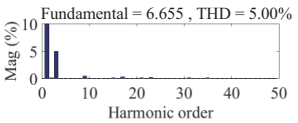

(d) FFT analysis of current at $M = 0.78$ (e) FFT analysis of current at $M = 0.7$

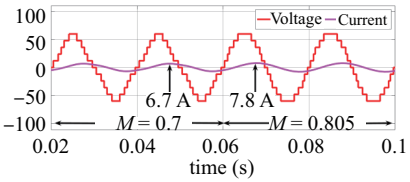

(f) voltage and current waveforms under change in $M = 0.7$ to 0.805

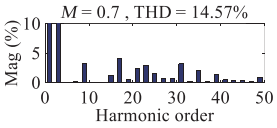

(g) FFT analysis at $M = 0.7$

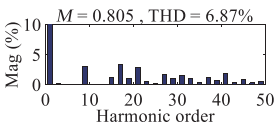

(h) FFT analysis at $M = 0.805$

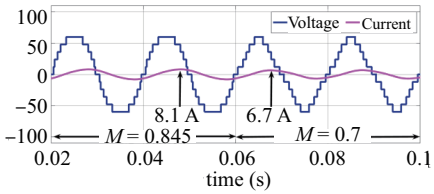

(i) voltage and current waveforms during sudden change in $M = 0.845$ to 0.7

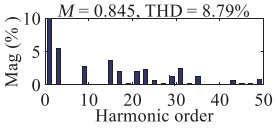

(j) FFT analysis at $M = 0.845$

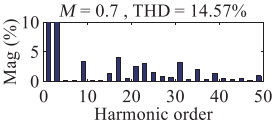

(k) FFT analysis at $M = 0.7$

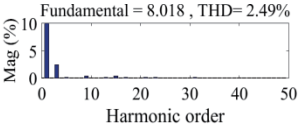

(l) FFT analysis at $M = 0.845$

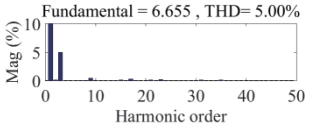

(m) FFT analysis at $M = 0.7$

Fig. 12. Simulation results of the proposed SHE method under dynamic change in M.

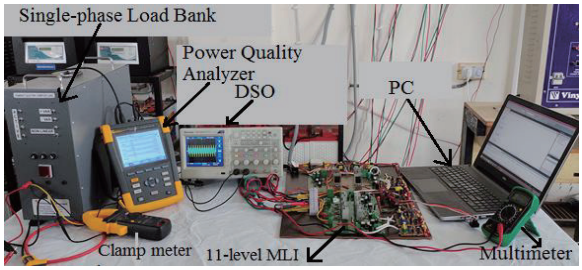

Fig. 13. Experimental setup of 11-level MLI.

TABLE V
HARDWARE SETUP SPECIFICATIONS

S.No.	Items	Quantity	Rating
1	Battery	05	12 V, 80 Ah
2	MOSFET, IRFP 460	12	500 V, 20 A
3	Gate driver, FOD 3180	12	2 A, Vcc ~(10-20 V)
4	Variable linear load bank (RL)	01	single-phase, 230 V, 1 kW
5	PCB	01	Single layer, 230 × 230 mm
6	Microcontroller, ATMEGA 32	01	8-bit AVR, 16 MHz clock frequency
7	AC/DC Converter (to fed power the gate drive circuit)	12	230 V / 12 V, 5 A
8	Power quality analyser, 435-II	01	3-phase supply, 1 V to 1000 V, resolution 0.01 V, 50 Hz
9	Digital oscilloscope, TDS2024C	01	4-channel, 200 MHz, Digital real-time sampling, up to 2 GS/s sample rate
10	11-Level Inverter	01	120 V, 20 A, 2 kW

analyzer, and PC is shown in Fig. 13. Table V shows the various components and their corresponding values used in the experimental case studies.

The switching angles computed by TSANR for a fixed M is converted into time instants t_1, t_2, t_3, t_4, and t_5 of microseconds. Using quarter-wave symmetry, a switching table is prepared for the complete cycle and these switching instants are fed to the ATMEGA 32 microcontroller, which simultaneously generates the switching pulses for the 11-level MLI. A dead-time of 10 μs is inserted between two complementary switches of the MLI. The proposed SHE method is implemented on the 11-level MLI for a resistive load of 8 Ω and an inductive load ($R = 5$ Ω, $L = 20$ mH).

The performance of the proposed method has been carried out based on two case studies: (1) under constant and (2) dynamic change in M.

A. Under Constant M

In this case study, the proposed SHE method is tested for different values of modulation indices. The experimental results measured for different modulation indices is shown in Fig. 13. The phase voltage and the current waveforms for the inductive load at $M = 0.8$ are shown in Fig. 14(a). It can be seen that the load voltage has 11 levels, while the current lags behind the voltage waveform with 0.62 power factor (p.f.). It

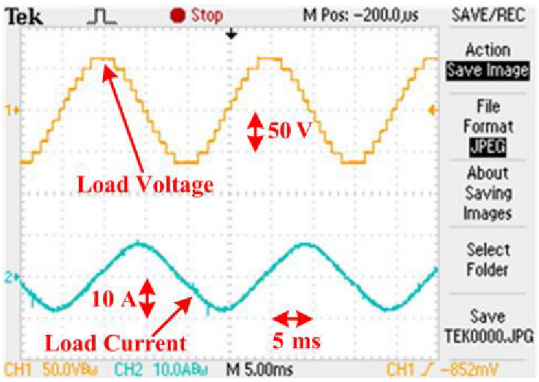

(a)

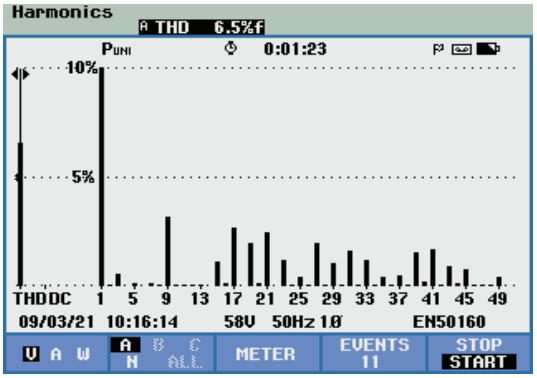

(b)

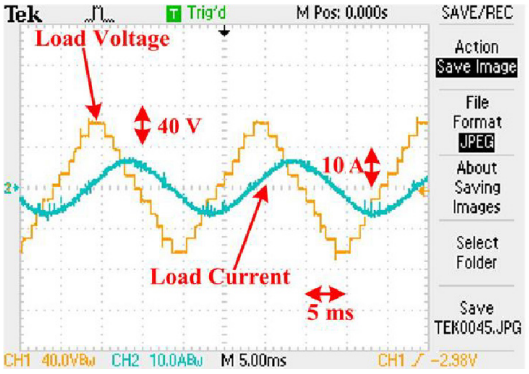

(c)

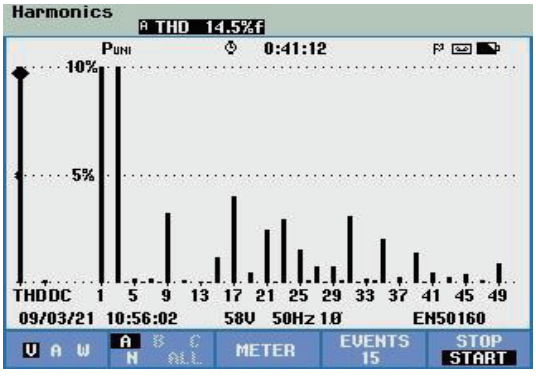

(d)

Fig. 14. Experimental results. (a) phase v and i waveforms at $M = 0.8$ with RL load, (b) harmonic plot of phase v at $M = 0.8$, (c) Phase v and i waveforms at $M = 0.7$ (RL load) and (d) Harmonic plot at $M = 0.7$.

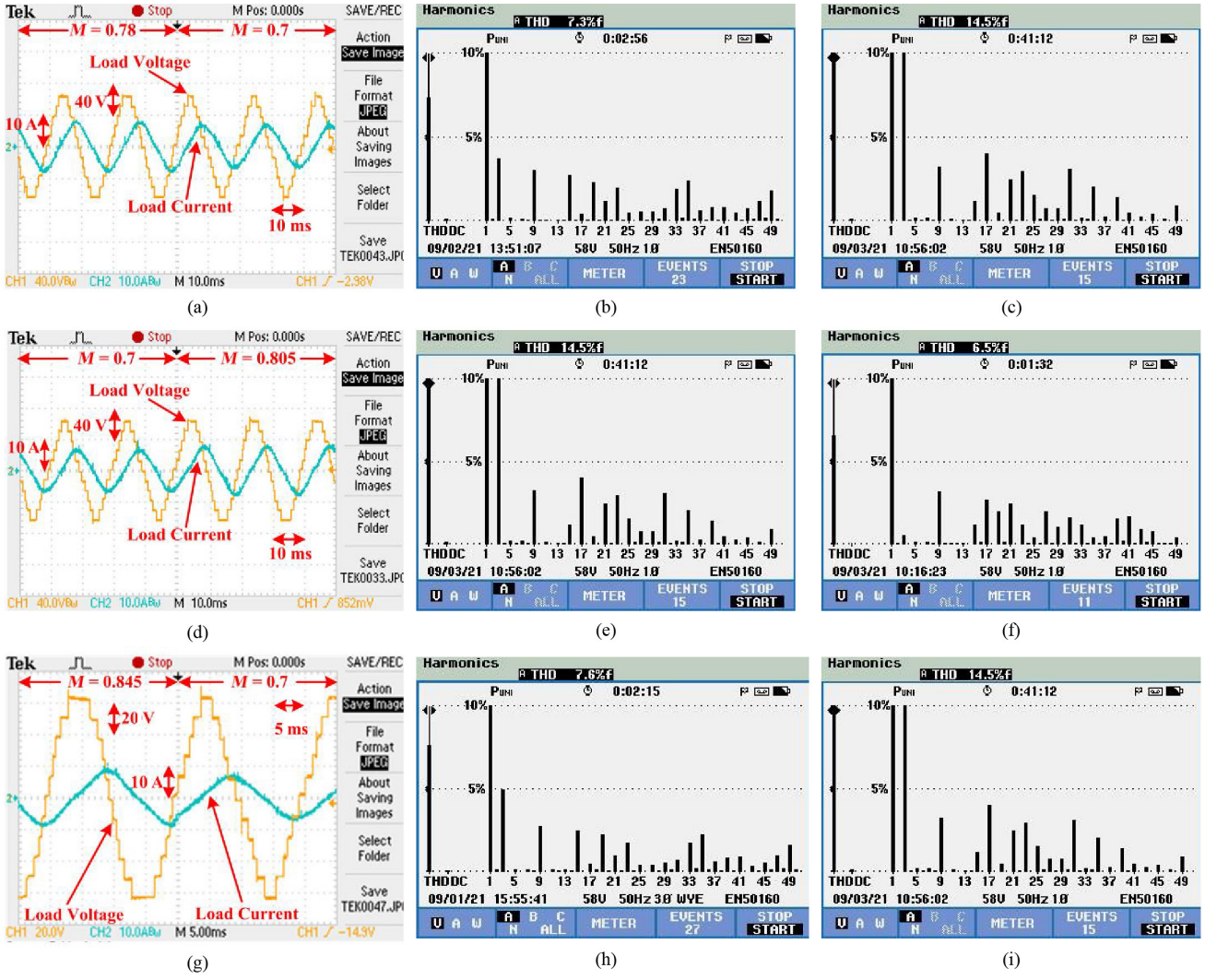

Fig. 15. Experimental results under dynamic change in modulation index (a) phase *v* and *i* waveforms with *M* varying from 0.78 to 0.7 for RL load, (b) harmonic plot of phase *v* at $M = 0.78$, (c) harmonic plot of phase *v* at $M = 0.7$, (d) phase *v* and *i* waveforms with *M* varying from 0.7 to 0.805 for RL load, (e) harmonic plot of phase *v* at $M = 0.7$, (f) harmonic plot of phase *v* at $M = 0.805$, (g) phase *v* and *i* waveforms with *M* varying from 0.845 to 0.7 for RL load, (h) harmonic plot of phase *v* at $M = 0.845$ and (i) harmonic plot of phase *v* at $M = 0.7$.

is evident that the current waveform approximates sine wave as inductive load suppresses the high order harmonics. The harmonic profile of the load voltage clearly demonstrates that the magnitude of the dominant 5th, 7th, 11th, and 13th harmonics are effectively suppressed as shown in Fig. 14(b). The THD of the phase voltage is measured at 6.5% and the actual RMS value is measured at 45.1 V, which is equal to the desired fundamental RMS voltage. Similarly, the load voltage and current waveforms and the harmonic analysis for $M = 0.7$ is shown in Fig. 14(c) and (d). The fundamental RMS load voltage and the THD is observed at 39.3 V and 7.6%, respectively.

B. Under Dynamic Change in M

In this case study, the proposed SHE method is tested under dynamic change in modulation index. Three test cases under dynamic change in M is considered to exhaustively validate the performance of the proposed SHE method.

Initially, the modulation index is decreased from $M = 0.78$ to 0.7 and the experimental waveform of the load voltage and current is shown in Fig. 15(a). Under dynamic change in *M*, the proposed TSANR SHE method quickly computes the new switching instants and mitigates the dominant order harmonics and the overall THD measured at $M = 0.78$ and 0.7 is 7.3% and 14.5%, respectively which is comparable to the simulation results as shown in Fig. 15(b) and (c). It is interesting to note that in the experimental results, the THD values are lower than the corresponding simulation results.

This is because the FFT analysis in MATLAB/Simulink consider harmonics up to 200th order which results in higher values of THD while in the experimental results harmonics up to 50th order is taken into consideration by the power quality analyzer.

In the second case, the modulation index is suddenly increased from $M = 0.7$ to 0.805 and the experimental waveform of the

TABLE VI
INDIVIDUAL HARMONICS FOR DIFFERENT MODULATION INDICES

M	Harmonics % (Simulation with dead-time)				Harmonics % (Experimental)			
	H_5	H_7	H_{11}	H_{13}	H_5	H_7	H_{11}	H_{13}
0.845	0.04	0.01	0.03	0.02	0.2	0.2	0.1	0.3
0.8	0.02	0.03	0.04	0.03	0.2	0.1	0.1	0.2
0.7	0.01	0.02	0.01	0.03	0.1	0.2	0.1	0.1
0.6	0.05	0.02	0.06	0.02	0.1	0.2	0.1	0.1
0.5	0.06	0.08	0.05	0.04	0.1	0.1	0.2	0.2
0.45	0.03	0.04	0.04	0.07	0.2	0.1	0.1	0.2

output voltage and current is shown in Fig. 15(d). The sudden increase in M results in the reduction in the overall THD of the output phase voltage from 14.5% to 6.5% is shown in Fig. 15(e) and (f). It is evident from Fig. 15(d), that there is an increase in the load current amplitude due to the increase in the amplitude of the fundamental phase voltage. Moreover, the dominant 5th, 7th, 11th and 13th order harmonics are minimized which reduces the overall THD of the load voltage at both $M = 0.7$ and 0.805.

In the final case, the modulation index is decreased from $M = 0.845$ to 0.7. The experimental waveform of the load voltage and current is shown in Fig. 15(g). Under sudden decrease in M, the load phase voltage is suddenly decreased which reduces the amplitude of the load current due to the decrease in the modulation index. The dominant harmonics are mitigated and the overall THD of the phase voltage is measured at 7.6% and 14.5% at $M = 0.845$ and 0.7, respectively as shown in Fig. 15(h) and (i).

Table VI shows the individual harmonics in simulation and experimental environment. The results shows that the individual harmonics are within the specified limit as per *IEEE standard 519-2022* [47].

The experimental results of the three test cases confirms that the proposed TSANR method quickly computes the new switching instants and exhibit negligible transients in the load voltage and current under dynamic change in M. It should be mentioned here that for high dimension SHE problem, the offline obtained firing angles occupies large memory storage and will not reach the new steady state under dynamic change in M. Hence, the proposed method is highly advantageous specially during online implementation and works well under fast sudden changes in M.

VIII. CONCLUSIONS

This paper proposed an initial solution based a fast convergence SHE method. It is shown that TSA quickly estimates the initial SHE solution as compared to the WO and GWO. This forms the basis of the proposed TSANR algorithm to obtain optimum final SHE solution for a wide range of M. A detailed comparative analysis is carried out on a five-dimensional SHE problem. This analysis showed that the proposed method computes the final SHE solution in 20 iterations with the highest accuracy. Furthermore, a comparison of the performance of the proposed SHE method with the state-of-the-art metaheuristic based SHE methods suggests that the proposed method significantly reduces the computational time in obtaining the accurate SHE solution ($f < 10^{-31}$). The simulation results indicate that the proposed TSANR method mitigates the dominant harmonics in the output phase voltage under sudden change in modulation index. Finally, the experimental results validate the efficacy of the proposed SHE method reduces the overall THD by effectively minimizing the 5th, 7th, 11th, and 13th order harmonics and the desired fundamental voltage is achieved under constant and dynamic change in modulation index.

The proposed SHE method can find numerous applications such as during V2G operation in electric vehicle, grid integration of distributed energy resources. As the modulation index will vary in grid connected applications specially during fault-ride-through condition, the proposed SHE method can be fruitful in reducing the overall THD and detrimental harmonics in the voltage waveform under dynamic change in modulation index. Since, the proposed SHE method targets to control fundamental and 5th, 7th, 11th, and 13th harmonic this will inevitably further increase the requirement of large memory space for the look up table. Moreover, the complexity of the proposed method is slightly higher due to dynamic change in modulation index which increases the overall hardware complexity as compared to the offline implementation of SHE method.

REFERENCES

[1] J. Rodriguez, J. S. Lai, and F. Z. Peng, "Multilevel inverters: A survey of topologies, controls, and applications," in *IEEE Transactions on Industrial Electronics*, vol. 49, no.4, pp. 724–38, Aug. 2002.

[2] C. Verdugo, J. I. Candela, F. Blaabjerg, and P. Rodriguez, "Three-phase isolated multimodular converter in renewable energy distribution systems," in *IEEE Journal of Emerging and Selected Topics in Power Electronics*, vol. 8, no. 1, pp. 854–865, Mar. 2020.

[3] P. Kala and S. Arora, "A comprehensive study of classical and hybrid multilevel inverter topologies for renewable energy applications," in *Renewable and Sustainable Energy Reviews*, vol. 76, pp. 905–931, Sept. 2017.

[4] M. S. A. Dahidah and V. G. Agelidis, "Selective harmonic elimination PWM control for cascaded multilevel voltage source converters: A generalized formula," in *IEEE Transactions on Power Electronics*, vol. 23, no. 4, pp. 1620–1630, Jul. 2008.

[5] S. Padmanaban, C. Dhanamjayulu, and B. Khan, "Artificial neural network and newton raphson (ANN-NR) algorithm based selective harmonic elimination in cascaded multilevel inverter for PV applications," in *IEEE Access*, vol. 9, pp. 75058–75070, May 2021

[6] M. S. A. Dahidah, G. Konstantinou, and V. G. Agelidis, "A review of multilevel selective harmonic elimination PWM: Formulations, solving algorithms, implementation and applications," in *IEEE Transactions on Power Electronics*, vol. 30, no. 8, pp. 4091–4106, Aug. 2015.

[7] K. Yang, Q. Zhang, R. Yuan, W. Yu, J. Yuan, and J. Wang, "Selective harmonic elimination with groebner bases and symmetric polynomials," in *IEEE Transactions on Power Electronics*, vol. 31, no. 4, pp. 2742–2752, Apr. 2016.

[8] S. Ahmad, A. Iqbal, M. Ali, K. Rahman, and A. S. Ahmed, "A fast convergent homotopy perturbation method for solving selective harmonics elimination pwm problem in multilevel inverter," in *IEEE Access*, vol. 9, pp. 113040–113051, Aug. 2021.

[9] M. Ahmed, M. Orabi, S. S. M. Ghoneim, M. M. Al-Harthi, F. A. Salem,

B. Alamri, and S. Mekhilef, "General mathematical solution for selective harmonic elimination," in *IEEE Journal of Emerging and Selected Topics in Power Electronics*, vol. 8, no. 4, pp. 4440–4456, Dec. 2020.

[10] M. A. Memon, S. Mekhilef, M. Mubin, and M. Aamir, "Selective harmonic elimination in inverters using bio-inspired intelligent algorithms for renewable energy conversion applications: A review," in *Renewable and Sustainable Energy Reviews*, vol. 82, no. 3, pp. 2235–2253, Feb. 2018.

[11] S. S. Lee, B. Chu, N. R. N. Idris, H. H. Goh, and Y. E. Heng, "Switched-battery boost-multilevel inverter with GA optimized SHEPWM for stand-alone application," in *IEEE Transactions on Industrial Electronics*, vol. 63, no. 4, pp. 2133–2142, Apr. 2016.

[12] A. Iqbal, M. Meraj, M. Tariq, K. A. Lodi, A. I. Maswood, and S. Rahman, "Experimental investigation and comparative evaluation of standard level shifted multi-carrier modulation schemes with a constraint GA based SHE techniques for a seven-level PUC inverter," in *IEEE Access*, vol. 7, pp. 100605–100617, 2019.

[13] M. Tarafdar Hagh, H. Taghizadeh, and K. Razi, "Harmonic minimization in multilevel inverters using modified species-based particle swarm optimization," in *IEEE Transactions on Power Electronics*, vol. 24, no. 10, pp. 2259–2267, Oct. 2009.

[14] H. Taghizadeh and M. Tarafdar Hagh, "Harmonic elimination of cascade multilevel inverters with nonequal DC sources using particle swarm optimization," in *IEEE Transactions on Industrial Electronics*, vol. 57, no. 11, pp. 3678–3684, Nov. 2010.

[15] A. Kavousi, B. Vahidi, R. Salehi, M. K. Bakhshizadeh, N. Farokhnia, and S. H. Fathi, "Application of the bee algorithm for selective harmonic elimination strategy in multilevel inverters," in *IEEE Transactions on Power Electronics*, vol. 27, no. 4, pp. 1689–1696, Apr. 2012.

[16] M. H. Etesami, N. Farokhnia, and S. Hamid Fathi, "Colonial competitive algorithm development toward harmonic minimization in multilevel inverters," in *IEEE Transactions on Industrial Informatics*, vol. 11, no. 2, pp. 459–466, Apr. 2015.

[17] M. H. Etesami, D. M. Vilathgamuwa, N. Ghasemi, and D. P. Jovanovic, "Enhanced metaheuristic methods for selective harmonic elimination technique," in *IEEE Transactions on Industrial Informatics*, vol. 14, no. 12, pp. 5210–5220, Dec. 2018.

[18] K. Haghdar, "Optimal DC source influence on selective harmonic elimination in multilevel inverters using teaching–learning-based optimization," in *IEEE Transactions on Industrial Electronics*, vol. 67, no. 2, pp. 942–949, Feb. 2020.

[19] K. P. Panda, P. R. Bana, and G. Panda, "FPA optimized selective harmonic elimination in symmetric–Asymmetric reduced switch cascaded multilevel inverter," in *IEEE Transactions on Industry Applications*, vol. 56, no. 3, pp. 2862-2870, May–Jun. 2020.

[20] A. Routray, R. Kumar Singh, and R. Mahanty, "Harmonic minimization in three-phase hybrid cascaded multilevel inverter using modified particle swarm optimization," in *IEEE Transactions on Industrial Informatics*, vol. 15, no. 8, pp. 4407–4417, Aug. 2019.

[21] K. P. Panda, S. S. Lee, and G. Panda, "Reduced switch cascaded multilevel inverter with new selective harmonic elimination control for standalone renewable energy system," in *IEEE Transactions on Industry Applications*, vol. 55, no. 6, pp. 7561–7574, Nov.–Dec. 2019.

[22] A. Routray, R. K. Singh, and R. Mahanty, "Harmonic reduction in hybrid cascaded multilevel inverter using modified grey wolf optimization," in *IEEE Transactions on Industry Applications*, vol. 56, no. 2, pp. 1827–1838, Mar.–Apr. 2020.

[23] J. Islam, S. T. Meraj, A. Masaoud, Md. M. Mahmud, A. Nazir, M. A. Kabir, Md. M. Hossain, and F. Mumtaz, "Opposition-based quantum bat algorithm to eliminate lower-order harmonics of multilevel inverters," in *IEEE Access*, vol. 9, pp. 103610–103626, Jul. 2021.

[24] P. Kala and S. Arora, "Implementation of hybrid GSA SHE technique in hybrid nine-level inverter topology," in *IEEE Journal of Emerging and Selected Topics in Power Electronics*, vol. 9, no. 1, pp. 1064–1074, Feb. 2021.

[25] M. A. Memon, M. D. Siddique, S. Mekhilef, and M. Mubin, "Asynchronous particle swarm optimization-genetic algorithm (APSO-GA) based selective harmonic elimination in a cascaded H-bridge multilevel inverter," in *IEEE Transactions on Industrial Electronics*, vol. 69, no. 2, pp. 1477–1487, Feb. 2022.

[26] Y. Li, X. -P. Zhang, and N. Li, "An improved hybrid PSO-TS algorithm for solving nonlinear equations of SHEPWM in multilevel inverters," in *IEEE Access*, vol. 10, pp. 48112–48125, Apr. 2022.

[27] G. Li, Z. Wu, D. Cao, and J. Li, "Random PWM selective harmonic elimination method with master-slave mode for seven-level MPUC inverter," in *CPSS Transactions on Power Electronics and Applications*, vol. 8, no. 1, pp. 87–96, Mar. 2023.

[28] R. Zhang, Z. Yin, J. Liu, and S. Yu, "Low carrier wave ratio modulation strategy of permanent magnet synchronous motor based on metro traction system: A comparative study," in *CPSS Transactions on Power Electronics and Applications*, vol. 7, no. 1, pp. 1–16, Mar. 2022.

[29] Y. Jiang, X. Li, C. Qin, X. Xing, and Z. Chen, "Improved particle swarm optimization based selective harmonic elimination and neutral point balance control for three-level inverter in low-voltage ride-through operation," in *IEEE Transactions on Industrial Informatics*, vol. 18, no. 1, pp. 642–652, Jan. 2022.

[30] M. Sadoughi, A. Pourdadashnia, M. Farhadi-Kangarlu, and S. Galvani, "PSO-optimized SHE-PWM technique in a cascaded H-bridge multilevel inverter for variable output voltage applications," in *IEEE Transactions on Power Electronics*, vol. 37, no. 7, pp. 8065–8075, Jul. 2022.

[31] M. Khizer, S. Liaquat, M. F. Zia, S. Kanukollu, A. Al-Durra, and S. M. Muyeen, "Selective harmonic elimination in a multilevel inverter using multi-criteria search enhanced firefly algorithm," in *IEEE Access*, vol. 11, pp. 3706–3716, Jan. 2023.

[32] S. Kundu and S. Banerjee, "An improved SHM-PAM technique for three-phase five-level CHB inverter utilizing both quarter-wave and half-wave symmetry waveforms to fulfill some important voltage harmonic standards," in *IEEE Transactions on Industry Applications*, vol. 57, no. 6, pp. 6246–6260, Nov.–Dec. 2021.

[33] M. Sharifzadeh, M. Babaie, G. Chouinard, K. Al-Haddad, R. Portill, L. G. Franquelo, and K. Gopakumar, "Hybrid SHM-PWM for common-mode voltage reduction in three-phase three-level NPC inverter," in *IEEE Journal of Emerging and Selected Topics in Power Electronics*, vol. 9, no. 4, pp. 4826–4838, Aug. 2021.

[34] L. Rosado, J. Samanes, E. Gubia, and J. Lopez, "Selective harmonic mitigation: Limitations of classical control strategies and benefits of model predictive control," in *IEEE Transactions on Industry Applications*, vol. 59, no. 5, pp. 6082–6094, Sept.–Oct. 2023.

[35] A. Moeini, S. Wang, B. Zhang, and L. Yang, "A hybrid phase shift-pulsewidth modulation and asymmetric selective harmonic current mitigation-pulsewidth modulation technique to reduce harmonics and inductance of single-phase grid-tied cascaded multilevel converters," in *IEEE Transactions on Industrial Electronics*, vol. 67, no. 12, pp. 10388–10398, Dec. 2020.

[36] S. A. Khan, D. Upadhyay, M. Ali, M. Tariq, A. Sarwar, R. K. Chakrabortty, M. J. Ryan, B. Alamri, and A. Alahmadi, "M-type and CD-type carrier based PWM methods and bat algorithm-based SHE and SHM for compact nine-level switched capacitor inverter," in *IEEE Access*, vol. 9, pp. 87731–87748, Jun. 2021.

[37] G. Schettino, C. Nevoloso, R. Miceli, A. O. D. Tommaso, and F. Viola, "Impact evaluation of innovative selective harmonic mitigation algorithm for cascaded H-bridge inverter on IPMSM drive application," in *IEEE Open Journal of Industry Applications*, vol. 2, pp. 347–365, Nov. 2021.

[38] J. Napoles, A. J. Watson, J. J. Padilla, J. I. Leon, L. G. Franquelo, P. W. Wheeler, and M. A. Aguirre, "Selective harmonic mitigation technique for cascaded H-bridge converters with nonequal DC link voltages," in *IEEE Transactions on Industrial Electronics*, vol. 60, no. 5, pp. 1963–1971, May 2013.

[39] M. Dabbaghjamanesh, A. Moeini, J. Kimball, and J. Zhang, "Using gated recurrent units for selective harmonic current mitigation-PWM in

grid-tied cascaded H-Bridge converters," in *IEEE Transactions on Industry Applications(Early Access)*.

[40] P. Kala and S. Arora, "Selective harmonic elimination in multilevel inverters using gravitational search algorithm," in *Proceedings of 2017 6th International Conference on Computer Applications* in *Electrical Engineering-Recent Advances (CERA)*, Roorkee, India, 2017, pp. 545–550.

[41] M. Ahmed, M. Orabi, S. S. M. Ghoneim, M. M. Al-Harthi, F. A. Salem, B. Alamri, and S. Mekhilef, "General mathematical solution for selective harmonic elimination," in *IEEE Journal of Emerging and Selected Topics in Power Electronics*, vol. 8, no. 4, pp. 4440–4456, Dec. 2020.

[42] S. Ahmad, A. Iqbal, M. Ali, K. Rahman, and A. S. Ahmed, "A fast convergent homotopy perturbation method for solving selective harmonics elimination PWM problem in multi level inverter," in *IEEE Access*, vol. 9, pp. 113040–113051, Aug. 2021.

[43] S. Kaur, L. K. Awasthi, A. L. Sangal, and G. Dhiman, "Tunicate swarm algorithm: A new bio-inspired based metaheuristic paradigm for global optimization," in *Engineering Applications of Artificial Intelligence*, vol. 90, p. 103541, Mar. 2020.

[44] S. Mirjalili, S. M. Mirjalili, and A. Lewis, "Grey wolf optimizer," in *Advances in Engineering Software*, vol. 69, pp. 46–61, 2014.

[45] S. Mirjalili and A. Lewis, "The whale optimization algorithm," in *Advances in Engineering Software*, vol. 95, pp. 51–67, 2016.

[46] Gui-Jia Su, "Multilevel DC-link inverter," in *IEEE Transactions on Industry Applications*, vol. 41, no. 3, pp. 848–854, May–Jun. 2005.

[47] IEEE Standard for Harmonic Control in Electric Power Systems, in *IEEE Std 519-2022 (Revision of IEEE Std 519-2014)* , vol., no., pp.1–31, 5 Aug. 2022.

Peeyush Kala was born in Pauri Garhwal, India, in April, 1987. He received the B.Tech. degree from Uttarakhand Technical University, Dehradun, India, in 2010, and the M.Tech. degree in electrical energy system and the Ph.D. degree in electrical engineering from the Govind Ballabh Pant University of Agriculture and Technology, Pantnagar, India, in 2012 and 2018, respectively. His employment experience included the work as an Assistant Professor in the Department of Electrical and Electronics Engineering, at Shivalik College of Engineering, Dehradun and the Department of Electrical Engineering, Women Institute of Technology, Dehradun, India, respectively. At present, he is working with the Department of Electrical and Electronics Engineering at SRM Institute of Science and Technology, Delhi-NCR Campus, Ghaziabad, India. His research interests include multilevel inverters, optimization techniques, and photovoltaic systems. He has published papers and book chapters in peer reviewed journals and conferences in the field of power electronics. He has completed one funded research project on development of hybrid multilevel inverter topology for distributed energy sources.

Abhinav Sharma received the B.Tech. degree from H. N. B. Garhwal University, Srinagar, India, in 2009, and the M.Tech. and Ph.D. degrees from Govind Ballabh Pant University of Agriculture and Technology, Pantnagar, India, in 2011 and 2016, respectively. He is currently working as an Assistant Professor (Selection Grade) with the Department of Electrical and Electronics Engineering, University of Petroleum and Energy Studies, Dehradun. He has published number of research articles in journals and conferences. His research interests include adaptive array signal processing, smart antennas, artificial intelligence, and machine learning.

Vibhu Jately received his Ph.D. degree from G. B. Pant University, Pantnagar, India. Following that, he worked as an Assistant Professor under United Nations Development Program within the Department of Electrical and Computer Engineering at Wollo University, Ethiopia. After that he worked as a Post-Doctoral Research Fellow for two years at MCAST Energy Research Group, Malta where he was a Task Leader of European H2020 projects. Currently he is working as an Assistant Professor (Selection Grade) in the Department of Electrical & Electronics Engineering at the University of Petroleum & Energy Studies, Dehradun, India. He has over eight years of teaching and research experience. His area of interest includes power electronics applications in renewable energy systems and has worked in formulating MPPT algorithms, control strategies for grid integration of PVs, microgrids and use of AI techniques in PV applications.

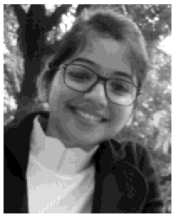

Jyoti Joshi received the B.Tech. degree in Electrical and Electronics Engineering from Uttarakhand Technical University (UTU), India, in 2011, and the M.Tech. degree from IFTM University, India, in 2015. She received her Ph.D. degree in Electrical Engineering from G. B. Pant University of Agriculture and Technology, Pantnagar. Currently she is working as an Assistant Professor within the Department of Computer Science and Engineer at Graphic Era Hill University, Dehradun. She has over eight years of teaching experience during which she also served as a Lecturer under United Nations Development Programme in Ethiopia. Her research interests include current controllers in grid-connected photovoltaic systems, fault ride through in grid-connected photovoltaic systems, and flexible power point tracking techniques in photovoltaic systems.

Yongheng Yang earned his B.Eng. degree in Electrical Engineering and Automation from Northwestern Polytechnical University, China, in 2009, and his Ph.D. degree in energy technology from Aalborg University, Denmark, in 2014. He pursued postgraduate studies at Southeast University, China, from 2009 to 2011 and was a Visiting Scholar at Texas A&M University, USA, during March-May 2013. From 2014 to 2020, he was associated with the Department of Energy Technology at Aalborg University, where he achieved the rank of tenured Associate Professor in 2018. In January 2021, he joined Zhejiang University in China as a ZJU100 Professor. He became a Zhejiang Kunpeng Investigator in 2023. His research focuses on gridintegration of photovoltaic systems and control of power converters, specifically grid-forming control technologies. Dr. Yang served as the Chair of the IEEE Denmark Section in 2019-2020 and is an Associate Editor for several IEEE Transactions. He received the 2018 IET Renewable Power Generation Premium Award and was recognized as an Outstanding Reviewer for the IEEE Transactions on Power Electronics in 2018. He was the recipient of the 2021 Richard M. Bass Outstanding Young Power Electronics Engineer Award from the IEEE Power Electronics Society (PELS) and the 2022 IEEJ Isao Takahashi Power Electronics Award. In addition, he has received two IEEE Best Paper Awards. He was included on the list of the Highly Cited Chinese Researchers by Elsevier in 2022-2023. He is presently a Vice Chair of the IEEE PELS Technical Committee on Sustainable Energy Systems and a Council Member of the China Power Supply Society.